SPECIAL SECTION PAPER

WILEY

Low-diffraction transparent micro light-emitting diode displays with optimized pixel structure

Qian Yang, SID Student Member[1] | Zhiyong Yang, SID Student Member[1] |
Yi-Fen Lan, SID Member[2] | Shin-Tson Wu, SID Fellow[1]

[1]College of Optics and Photonics, University of Central Florida, Orlando, Florida, USA

[2]AU Optronics Corp., Hsinchu, Taiwan

Correspondence
Shin-Tson Wu, College of Optics and Photonics, University of Central Florida, Orlando, FL, USA.
Email: swu@creol.ucf.edu

Abstract

Transparent displays suffer from background image blur due to light diffraction when passing through periodic pixel structures. A simple, reference-image free and semi-analytical model based on diffraction theory and human eye's angular resolution is proposed to quantitatively evaluate the diffraction effect of transparent displays. Several factors including object distance, resolution and aperture ratio are analyzed with our model to establish guidelines for minimizing the diffraction effect in transparent displays. By optimizing the pixel structures within a 2×2-pixel size region, the relative diffraction intensity is reduced by 42% at the 50% aperture ratio regardless of pixel density, which is valuable for achieving diffraction-less high resolution and low aperture ratio transparent displays with current fabrication technologies.

KEYWORDS

diffraction suppression, micro-LED, pixel structure optimization, transparent display, under-display camera

1 | INTRODUCTION

Transparent display is a promising technology with potential applications in smart windows, automotive windshield displays, Under-Display Cameras, Under-Display Sensors, and augmented reality displays for showcase,[1,2] to name a few. The emerging μLED (micro light-emitting diode) technology[3–5] is a promising solution for transparent displays because of its high brightness and large aperture ratio due to the small chip size and inorganic emissive nature.[6] Sony has successfully developed a tiled 16K μLED screen with 99% aperture ratio,[7] which shows an outstanding ambient contrast ratio (ACR), although the pixel per inch is only about 20. For AR automotive applications, clear and vivid images from display itself (foreground) and the scene after display (background) are both desired. Also, high illuminance and high ACR are necessary for outdoor scenarios.[8] Conventional projection type head up displays

(HUDs) adopt a more complex system design including a light engine, reflective mirrors, and an optical combiner.[9,10] With a transparent display on the windshield, a much simpler system design can be realized for a monoscopic AR display.[11] Moreover, due to inherent transparency and self-illumination, higher optical efficiency, wider color gamut, larger eyebox and field of view (FoV) can be expected in a transparent HUD. Compared with μOLED,[12,13] μLED does not have the tradeoff between high illuminance and lifetime, which suggests that the μLED chip size can be smaller for achieving a higher transparency. Yet, in a transparent μLED display, the see-through images are often blurred caused by light diffraction after passing through the periodic pixel structures.[14] Our study shows that the image quality deteriorates more if the objects are far away from the display panel, which is a common situation while driving.

For smartphone applications, manufacturers are pursuing bezel-less, full-screen designs with high pixel

density to enhance the interaction between users and devices. Under-display camera is a new trend to achieve a sleek industrial design but mounting the display in front of a camera will also cause severe image degradation. Deep learning related algorithms are adopted to restore the blurred images by modeling different optical effects caused by the display, camera lens and human vision system, but real-time algorithms are hard to be applied in preview and video mode currently.[15] Thus, it is of great importance to suppress the diffraction effect from the optics viewpoint, especially for high pixel density devices where a high aperture ratio is difficult to achieve.

Transparent display is essentially a binary aperture function from the viewpoint of diffraction theorem, where the transmittance is 1 in open regions and 0 in opaque regions. Tsai et al.[16] studied the diffraction widths with a Gaussian beam passing through apertures with different pixel structures and assumed that a narrower diffraction width could mitigate the diffraction effect. This assumption does not take human factors into account so that the result might lead to some uncertainty due to the finite aperture size (on the order of millimeters). Qin et al.[17] proposed to simulate diffracted see-through images and evaluate the pixel structures with subjective image quality score. To our knowledge, no simple, reference-image independent and physically intuitive evaluation methodology is proposed for the diffraction effect of transparent displays with human factors considered. In this paper, we first build our quantitative evaluation method for the diffraction effect perceived by human eyes and then analyze the magnitude of diffraction in a conventional pixel structure with various object distances, resolutions, and aperture ratios. A pixel structure optimization method is introduced to minimize the

diffraction effect for transparent displays with a small aperture ratio.

2 | THEORY

The point spread function (PSF) is the response of an incoherent imaging system to an input point source, while the blurred images can be obtained by convolution of the objects and the PSF. Thus, by studying the PSF of an imaging system including a transparent display and a human eye, one can investigate the diffraction effect of pixel structures. Figure 1 shows the schematics of the imaging system, where the light from background objects propagates in free space for d_1 before passing through the transparent display. A human eye is modeled as a positive lens with focal length f, positioned at d_2 after the transparent display, U_1 is a virtual plane immediately in front of the lens to assist in the derivation, and the imaging plane (U_2) is located on the retina.

The derivation of the monochromatic PSF with a finite object distance d_1 has been reported in Qin et al.[17] and the system PSF on the retina can be expressed as follows:

$$ \mathrm{h}(x,y) \propto \left| \mathbf{F}\{\mathrm{t}(\xi,\eta)\} \right|_{f_x=\frac{x}{\lambda M f}, \ f_y=\frac{y}{\lambda M f}} \bigg|^2, \tag{1} $$

where f_x and f_y is the spatial frequency in x and y direction, respectively, λ is the wavelength, and script letter F is the symbol for Fourier transform (FT). In Equation 1, the finite pupil size of human eye is ignored since this study focuses on the diffraction from display panel. In this imaging system, the PSF $h(x,y)$ is the
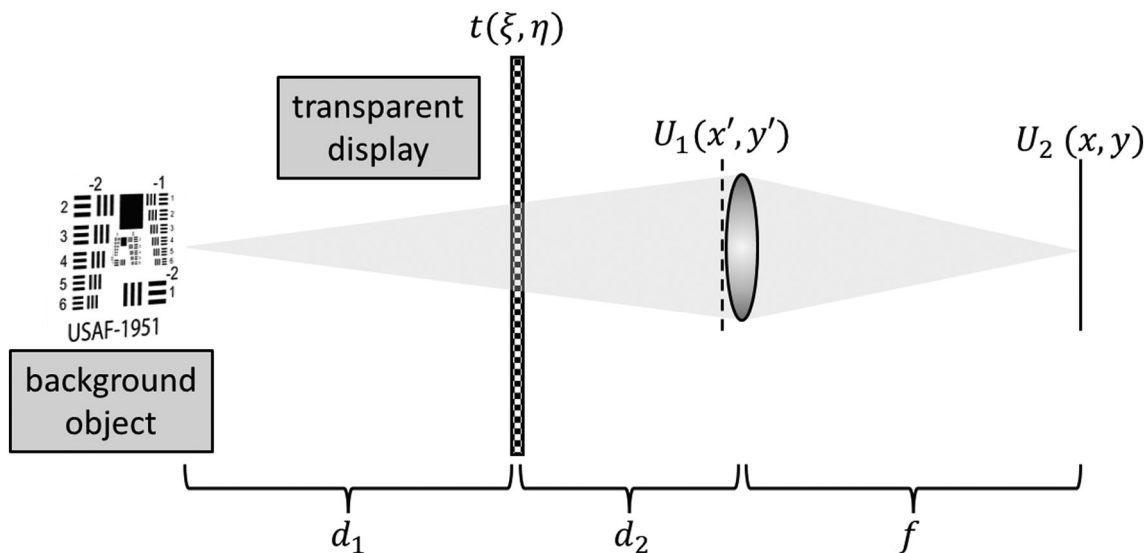

FIGURE 1 Schematics of the imaging system

modulus square of FT of the aperture distribution $t(\xi,\eta)$. The human eye acts as a lens and the retina as the receiver plane. The optical power of human eye can be dynamically adjusted to satisfy the object-image relation, approximated by the Gaussian optics[18] in Equation 2, following the convention in a Cartesian coordinate system,

$$\frac{1}{s_o} + \frac{1}{s_i} = \frac{1}{f} \tag{2}$$

where s_i and s_o are the image and object distances, and f is the focal length of the eye. In human eyes, the image distance can be regarded as the distance between pupil and retina, which is about 17 mm. In Figure 2, the focal length of the eye is plotted as a function of the object distance. When the object distance is 30 cm, the focal length is about 16 mm, which suggests that treating the focal plane as the imaging plane is a good approximation for any object distance farther than 30 cm. We choose focal length $f = 17$ mm in the following simulations.

Parameter $M = d_1/(d_1 + d_2)$ is a metric for relative object distance from the transparent display and $M = 1$ when the object is at infinity. The transparent display is regarded as a 2D aperture function $t(\xi,\eta)$, where amplitude transmittance is defined as either 0 (*opaque*) or 1 (*transparent*) at each point. The opaque area includes the emitting unit and the circuits, and the rest area is transparent. In Fourier optics, the display panel with periodic pixel arrangement can be modeled as a 2D grating as it redistributes the incident light into various diffraction orders. Therefore, following the convention in Goodman,[14] the aperture function $t(\xi,\eta)$ can be modeled by convolution between a unit cell function $t_0(\xi,\eta)$ and a comb function and constrained by finite boundaries

FIGURE 2   Focal length f of the eye as a function of object distance

represented by a rectangular function, as shown in Equation 3,

$$t(\xi,\eta) = \left[t_0(\xi,\eta) \otimes \mathrm{comb}\left(\xi/L_{x_0}, \eta/L_{y_0}\right)\right] \tag{3}$$
$$\times \mathrm{rect}(\xi/L_x)\mathrm{rect}\left(\eta/L_y\right),$$

where L_{x0} and L_{y0} are the size of the unit cell, and L_x and L_y are the actual size of the display panel. Its FT can be expressed as follows:

$$h(x,y) \propto \left| \left[h_0\left(f_x, f_y\right) \times \mathrm{comb}\left(L_{x_0}f_x, L_{y_0}f_y\right) \right] \right.$$
$$\left. \otimes \mathrm{sinc}(L_xf_x)\mathrm{sinc}\left(L_yf_y\right) \right|^2_{f_x=\frac{x}{\lambda Mf}, f_y=\frac{y}{\lambda Mf}}, \tag{4}$$

where $h_0(f_x,f_y)$ is the FT of $t_0(\xi,\eta)$.

In Figure 3, an intuitive demonstration of how to efficiently calculate the system PSF is illustrated, where the FT of unit cell function $t_0(\xi,\eta)$ can be solved first and then PSF $h(x,y)$ is analytically obtained. Due to the complex aperture structure, sometimes the analytical derivation is not possible and numerical simulation is performed with the aid of fast FT (FFT) algorithm. In this way, tremendous computational load is greatly relieved, while accurate PSF is still guaranteed. If the physical size of the unit cell is set to be $L_{0x} \times L_{0y}$ and sampling points are $N_x \times N_y$, then the physical size on the receiver plane should be $N_xM\lambda f/L_{x0} \times N_yM\lambda f/L_{y0}$. The comb function in PSF expression indicates the spacing between diffraction orders on the retina is $M\lambda f/L_{x0}$ and $M\lambda f/L_{y0}$ in x and y direction and the sinc function means that each diffraction order has a finite diffraction width $M\lambda f/L_x$ and $M\lambda f/L_y$. The angular resolution of human eye is 1 arcminute and its corresponding length on the retina is 5 μm. Since the energy mainly concentrates in the zeroth diffraction order, located in the center of imaging plane, and gradually decreases in the higher orders, it is reasonable to assume that only diffraction orders that are 5 μm away from the zeroth order can be distinguished by the eye. Those closer diffraction orders are blended with zeroth order, indistinguishable to human eye. Therefore, a relative diffraction intensity, defined as maximum diffraction intensity outside the 5-μm region to the zeroth order intensity, is used to quantitatively characterize the diffraction effect of transparent display to human eye. The diffraction width of the sinc function is about tens of nanometers or less for a display panel with 10^3–10^4 pixels in each dimension, which is relatively small compared with human eye resolution and thus can be ignored in the PSF calculation. That means the system PSF can be simplified as a comb function modulated by FT of unit cell function $t_0(\xi,\eta)$.
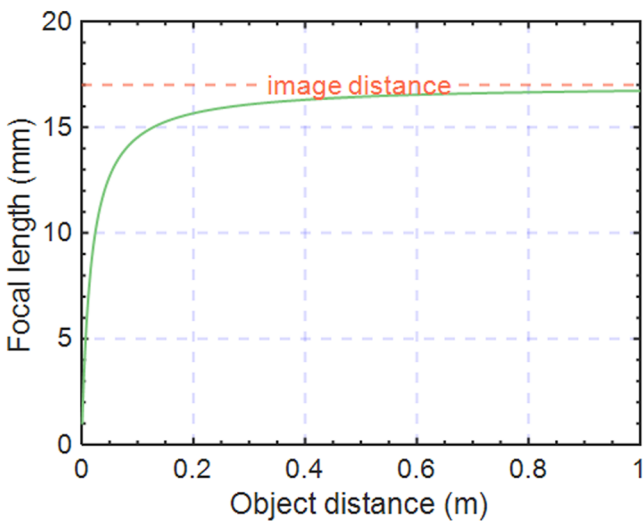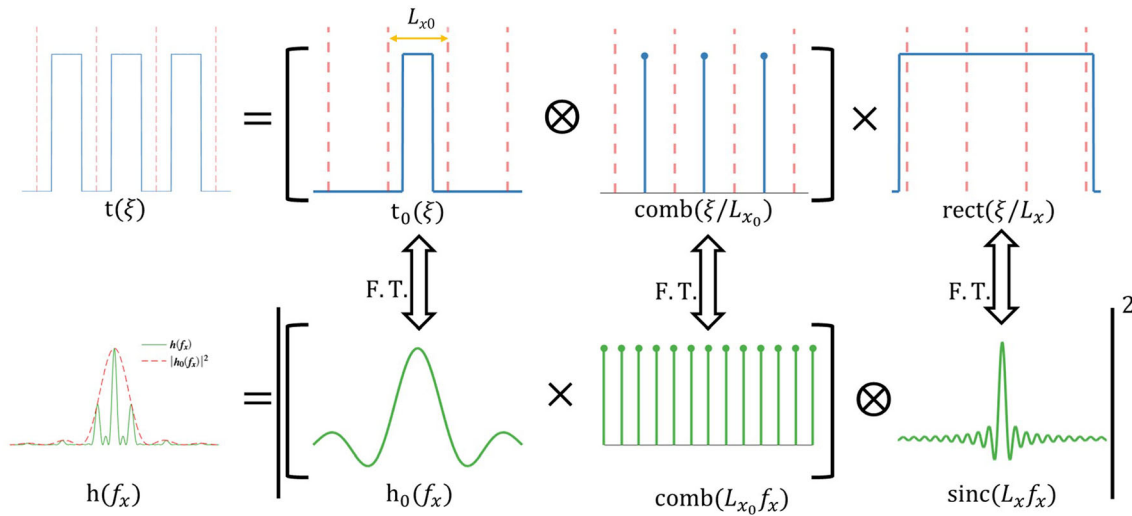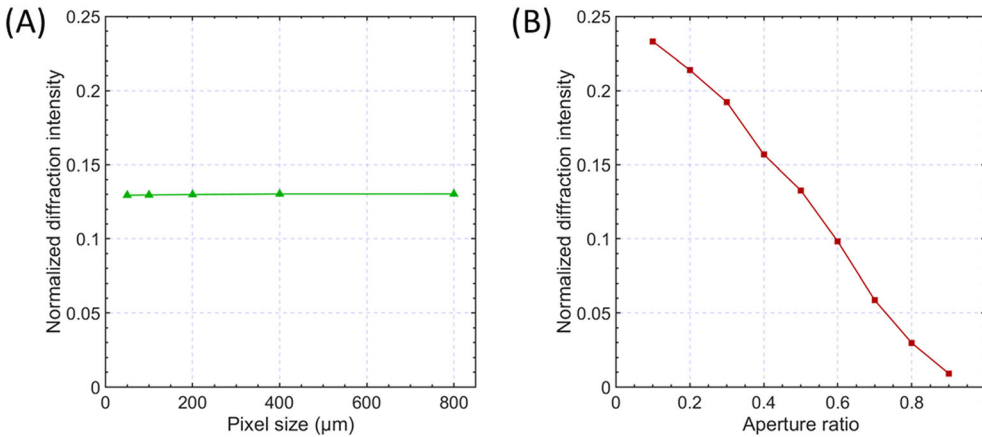
FIGURE 3 A visual representation of point spread function (PSF) calculation in an imaging system including a transparent display. For simplicity, 1D derivation is shown here but it is easy to extend to two dimensions

FIGURE 4 (A) At aperture ratio $\alpha = 50\%$, the relative diffraction intensity is invariant to the pixel size $p = 50$–800 µm. (B) With pixel size $p = 400$ µm, the relative diffraction intensity decreases as aperture ratio α increases from 10% to 90%

3 | CONVENTIONAL PIXEL STRUCTURES

In conventional pixel structures, the positions of the opaque region in each pixel are the same. The impact of object distance, panel resolution, and pixel aperture ratio on the diffraction effect to human eye is analyzed by our model. Without losing generality, we assume the pixel geometry is square with side length p and the opaque region geometry is also square, located in the center of each pixel, since the diffraction effect is found to be irrelevant to pixel/opaque geometry.[17] Unlike the definition in Huang et al.,[3] here the aperture ratio α represents the area of transparent region to that of the pixel. The side length of opaque region b is determined by the aperture ratio α, proportional to the square root of 1-α. Noticing that the spacing between diffraction orders is proportional to the parameter M. If M is small, the PSF is scaled down and most energy is within 5 µm from the zeroth

diffraction order so that the diffraction effect is negligible. Hence, the diffraction effect is most obvious when the object is at infinity ($M = 1$) and the following analyses are taken under this extreme scenario.

The panel resolution is determined by the pixel size. For common display devices, the pixel size ranges from tens of microns (smartphones) to hundreds of microns (TVs). In Figure 4A, the aperture ratio is set at $\alpha = 50\%$ and the relative diffraction intensity is invariant to the pixel size. This result seems counter-intuitive at the first glance because diffraction effect is generally more obvious with finer structure, but it coincides with the conclusion in Qin et al.,[17] by evaluating the subjective score of see-through images. From Equation 3, the pixel size only impacts the coordinate transformation in the PSF calculation and the diffraction order spacing is inversely proportional to the pixel size. Even with an unrealistically large pixel size $p = 1000$ µm, the order spacing is 9.35 µm at a green light ($\lambda = 550$ nm). Since the diffraction order

spacings are larger than human eye's angular resolution, the same diffraction intensity is observed by human.

Another important impact factor is the aperture ratio. In Figure 4B, the pixel sizes are set to be 400 μm, and the relative diffraction intensity decreases as the aperture ratio increases from 10% to 90%. According to the similarity theorem of FT, the open region is stretched at a higher aperture ratio and its PSF is squeezed, leading to a lower diffraction intensity. It seems that boosting the aperture ratio of pixels is the only way to suppress diffraction effect in the conventional pixel structures. The aperture ratio is directly related to the chip size of the employed LED.

However, even with μLED technology, it is still difficult to achieve a large aperture ratio while maintaining high resolution with current fabrication technologies. It would be of practical interest for smartphone applications if the diffraction effect could be reduced even at a small aperture ratio.

4 | OPTIMIZED PIXEL STRUCTURES

In Figure 3, the size of unit cell function $t_0(\xi,\eta)$ is the same as the pixel size, but in fact the unit cell could
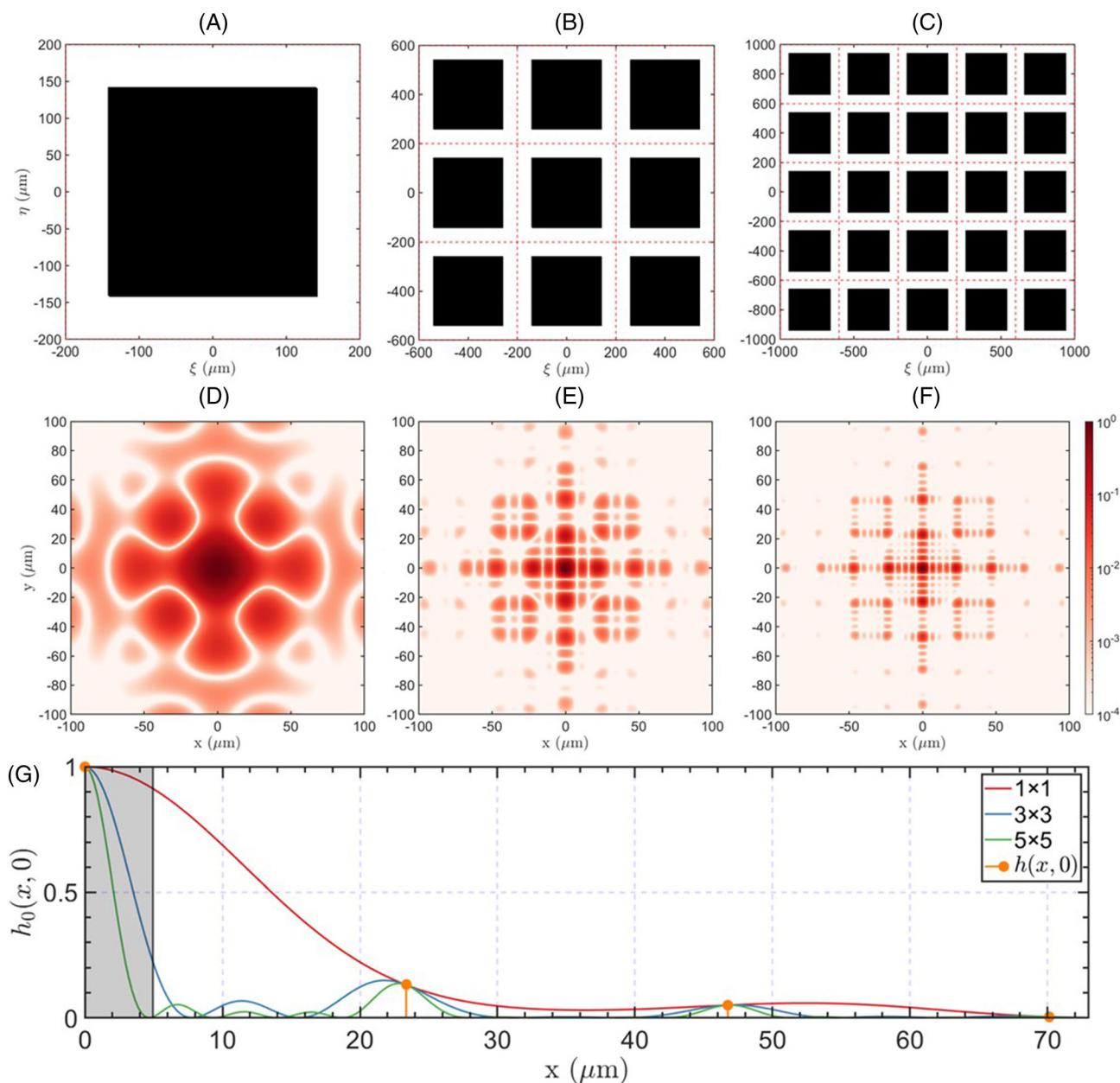

FIGURE 5 (A–C) With pixel size $p = 400$ μm and aperture ratio $\alpha = 50\%$, unit cell functions $t_0(\xi,\eta)$ with 1×1, 3×3, 5×5 pixels in one unit cell for conventional pixel structures. (D–F) Fourier transforms (FTs) of unit cell functions in (A)–(C). (G) The horizontal cross-section $h_0(x,y)$ excerpted from (D)–(F)

include more pixels and final PSF will be the same for conventional pixel structures. With $p = 400$ μm and $\alpha = 50\%$, Figure 5A–C shows the $t_0(\xi,\eta)$ with 1×1, 3×3, 5×5 pixels in one unit cell, respectively, and their FT $h_0(x,y)$ in Figure 5A–C looks quite different. Figure 5F shows their horizontal cross section $h_0(x,0)$, and they all converge to the same PSF $h(x,0)$ after multiplying by comb functions with corresponding diffraction order spacing. After all, in conventional pixel structures, the choice of unit cell only affects how we represent the same aperture function $t(\xi,\eta)$ mathematically and their PSFs remain the same physically. Nevertheless, it is enlightening that optimizing the pixel structures within a unit cell $t_0(\xi,\eta)$ containing several pixels could possibly decrease the diffraction intensity. Here, the coordinates of the opaque regions in each pixel are the optimization variables, and the diffraction intensity is the objective functions. The vertical coordinates in each row and horizontal coordinates in each column should stay the same for the ease of circuit layout and fabrication. This restriction greatly reduces the optimization variables from $2n^2$ to $2n$ for a unit size with $n \times n$ pixels.

In the global optimization, the unit cell sizes are set by pixel number in one dimension $n = 1$–10 and the aperture ratios are set at $\alpha = 30\%$, 50%, and 70%. The optimized diffraction efficiency at each case is plotted in Figure 6. As the pixel number n increases, the diffraction efficiency decreases and gradually converges to a stable value for each aperture ratio. Before optimization, the
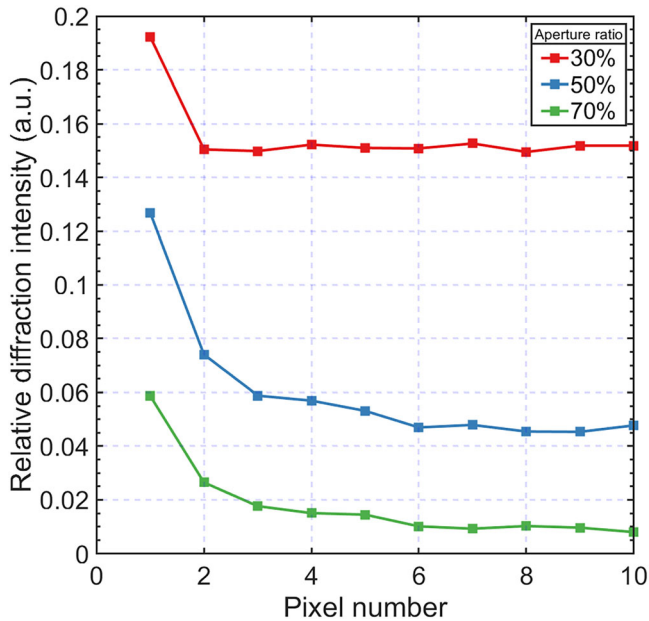

FIGURE 6 Global optimization result of diffraction intensities with unit cell sizes $n = 1$–10 and aperture ratios $\alpha = 30\%$, 50%, and 70%

diffraction intensity for each aperture ratio is 0.19, 0.13, and 0.06, respectively, and it drops to 0.15, 0.05, and 0.01 after optimization, where the relative diffraction intensity drop is 21%, 62%, and 83%. When pixel number $n = 1$, the diffraction intensities are the same as those in an unoptimized structure due to periodicity. The diffraction intensity of an optimized pixel structure with $\alpha = 50\%$ is even lower than that of an unoptimized $\alpha = 70\%$ structure. By optimizing pixel structures in unit cells with $n = 2$, the diffraction effect has been greatly mitigated, and the relative diffraction drops are 21%, 42%, and 58% at each aperture ratio. One of the optimized cell unit pixel structures $t_0(\xi,\eta)$ for $n = 3$ and $\alpha = 50\%$ is shown in Figure 7A and its FT $h_0(x,y)$ and horizontal cross section $h_0(x,0)$ is plotted in Figure 7B,C. Compared with the unoptimized structure, the energy distribution in the optimized pixel structure avoids its peaks to be coincided with the position of diffraction orders, leading to an effectively lower diffraction intensity. This result can also be extended to smaller pixels if the relative coordinates of the opaque region in each pixel are considered as the optimization variables.

With the aid of PSF, the diffracted images of background objects could be obtained by convolution, assuming the display panel is viewed on-axis. It should be noticed that the PSF is wavelength dependent, thus monochromatic PSFs for each individual wavelength are essential for a RGB full-color object. For simplicity, the background objects are treated as a gray-level 2D image with a uniform reflective spectrum illuminated by a D65 light source. Before implementing the convolution, the gray-level image should be resized to maintain the same physical length at each wavelength. After the convolution, the image should be interpolated again to have the same sampling points. As in the hyperspectral imaging, the data on the receiver plane after the convolution is a stacked 2D intensity, where each pixel has its own spectrum distribution. For visualization, the spectrum information is converted to *XYZ* tristimulus value first, as in Equation 5:

$$
\begin{aligned}
X &= k \sum_{\lambda=380\text{nm}}^{\lambda=780\text{nm}} E(\lambda)x(\lambda)P(\lambda), \\
Y &= k \sum_{\lambda=380\text{nm}}^{\lambda=780\text{nm}} E(\lambda)y(\lambda)P(\lambda), \\
Z &= k \sum_{\lambda=380\text{nm}}^{\lambda=780\text{nm}} E(\lambda)z(\lambda)P(\lambda),
\end{aligned}
\tag{5}
$$

where $E(\lambda)$ is the illumination source, $P(\lambda)$ is the intensity distribution, $x(\lambda)$, $y(\lambda)$, and $z(\lambda)$ are the CIE 1931 2-degree color-matching functions and k is a normalization factor. For RGB values, we choose sRGB system to perform the conversion, using the transformation matrix shown in Equation 6:
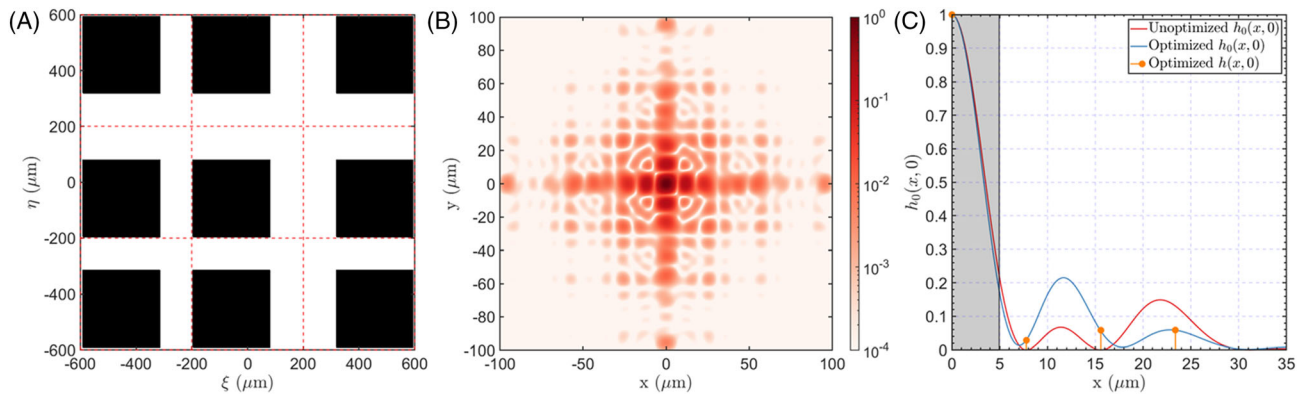
FIGURE 7 (A) An optimized pixel structures within a unit cell with 3×3-pixel size and aperture ratio $\alpha = 50\%$. (B) Fourier transform (FT) of the optimized structure. (C) Horizontal cross section $h_0(x,0)$ of the optimized and unoptimized structures and PSF $h(x,0)$ of the optimized structure

FIGURE 8 (A) Test background object. (B) Diffracted image with an unoptimized pixel structure at 30% aperture ratio
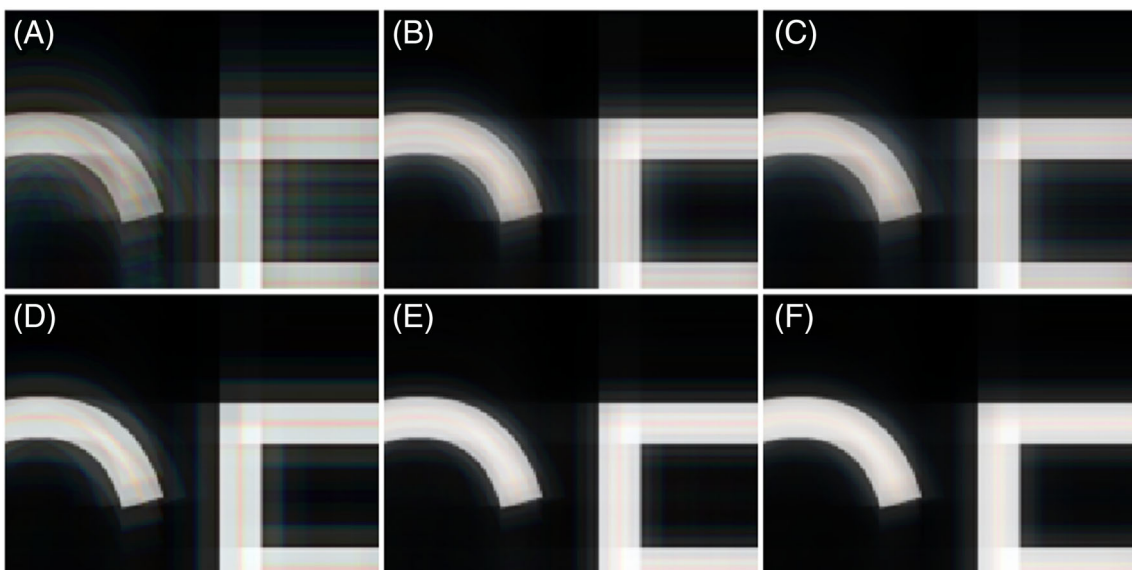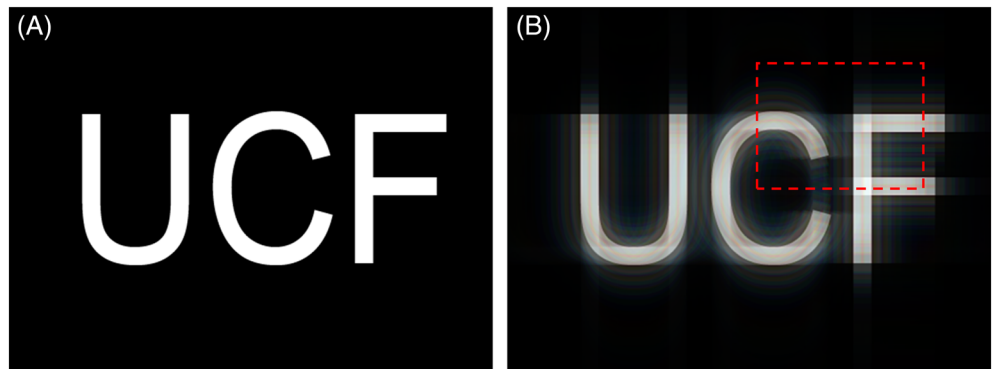
FIGURE 9 Diffracted images at aperture ratio 30% (A–C) and 50% (D–F) with unit cell sizes $n = 1,2,3$

$$T_{XYZ \to RGB} = \begin{bmatrix} 3.2404542 & -1.5371385 & -0.4985314 \\ -0.9692660 & 1.8760108 & 0.0415560 \\ 0.0556434 & -0.2040259 & 1.0572252 \end{bmatrix},$$
(6)

And a gamma correction Equation 7 is performed for the computer display:

$$V = \begin{cases} 12.92v & \text{if } v \le 0.0031308 \\ 1.055v^{\frac{1}{2.4}} - 0.055 & \text{otherwise} \end{cases},$$
(7)

where v is the linear sRGB value and V is the nonlinear sRGB value. The *XYZ* values and RGB values in the calculation are forced to be in the range within 0–1, by simple clipping method where the values above 1 are suppressed to 1 and those below 0 are replaced by 0. If the values greatly exceed 1, perhaps a scaling method is preferable. The accuracy of this method has been experimentally verified in Qin et al.[17] To intuitively illustrate the diffraction-suppression effect of our optimized pixel structures, three letters "UCF" are used as background object, shown in Figure 8A. We assume $d = 25$ cm and the object size is 50 mm × 38 mm, located at 1-m away from the observer. Image blur effect with unoptimized structure is displayed in Figure 8B. Figure 9 shows the improved image quality with our optimized pixel structures. The diffraction is greatly suppressed with a 2×2-pixel unit cell, comparing Figure 9D with Figure 9E.

5 | CONCLUSION

We have established a simple and reference image independent model to quantitatively evaluate the diffraction effect of transparent displays. Based on diffraction theory, the PSF of the imaging system including the transparent display aperture function and human eye is derived, and the relative diffraction intensity is used as the metric to characterize the diffraction effect by considering the angular resolution of human eyes. The impact of object distance, panel resolution, and pixel aperture ratio to the diffraction intensity is analyzed in the conventional pixel structures. As a result, the object at infinity suffers the most from diffraction. A larger aperture significantly reduces the diffraction intensity, while the resolution plays a trivial role. The aperture function of the transparent display is regarded as a 2D grating, which can be segmented as the convolution of a unit cell function and a comb function. By optimizing the pixel structures within unit cells with 2×2-pixel size, the relative diffraction intensity drops 42% at the 50% aperture ratio, equivalent to that of the unoptimized pixel structure with 70% aperture ratio. Our proposed method is simple, yet it opens a new way to suppress the diffraction effect for a transparent display by slightly tweaking the pixel structure. Especially, large aperture ratio and high pixel density panels are still difficult to achieve simultaneously with current fabrication capability.

ORCID
Qian Yang https://orcid.org/0000-0003-3630-3559
Zhiyong Yang https://orcid.org/0000-0002-7181-7443
Shin-Tson Wu https://orcid.org/0000-0002-0943-0440

REFERENCES
1. Wager JF. Transparent electronics. Science. 2003;300(5623): 1245–6.
2. Xiong J, Hsiang EL, He Z, Zhan T, Wu ST. Augmented reality and virtual reality displays: emerging technologies and future perspectives. Light Sci Appl. 2021;10(1):216.
3. Huang Y, Hsiang EL, Deng MY, Mini-LED WST. Micro-LED and OLED displays: present status and future perspectives. Light Sci Appl. 2020;9(1):105.
4. Cok RS, Meitl M, Rotzoll R, et al. Inorganic light-emitting diode displays using micro-transfer printing. J Soc Inf Disp. 2017;25(10):589–609.
5. Huang Y, Tan G, Gou F, Li MC, Lee SL, Wu ST. Prospects and challenges of mini-LED and micro-LED displays. J Soc Inf Disp. 2019;27(7):387–401.
6. Liu YT, Liao KY, Lin CL, Li YL. 66-2: invited paper: PixeLED display for transparent applications. SID Int Symp Dig Tech Pap. 2018;49(1):874–5.
7. Biwa G, Aoyagi A, Doi M, Tomoda K, Yasuda A, Kadota H. Technologies for the Crystal LED display system. J Soc Inf Disp. 2021;29(6):435–45.
8. Lee YH, Zhan T, Wu ST. Prospects and challenges in augmented reality displays. Virtual Real Intell Hardw. 2019;1(1):10–20.
9. Kim H, Miranda Anon A, Misu T, Li N, Tawari A, Fujimura K. Look at me: augmented reality pedestrian warning system using an in-vehicle volumetric head up display. Proceedings of the 21st International Conference on Intelligent User Interfaces. 2016;294–8.
10. Huang Y, Liao E, Chen R, Wu ST. Liquid-crystal-on-silicon for augmented reality displays. Appl Sci. 2018;8(12):2366.
11. Gabbard JL, Fitch GM, Kim H. Behind the glass: driver challenges and opportunities for AR automotive applications. Proc IEEE. 2014;102(2):124–36.
12. Krotkus S, Kasemann D, Lenk S, Leo K, Reineke S. Adjustable white-light emission from a photo-structured micro-OLED array. Light Sci Appl. 2016;5(7):e16121.
13. Chen KT, Huang YH, Tsai YH, et al. 60-1: invited paper: highly transparent AMOLED display with interactive system. SID Int Symp Dig Tech Pap. 2019;50(1):842–5.

14. Goodman JW. Introduction to Fourier Optics Roberts and Company Publishers; 2005.

15. Zhou Y, Ren D, Emerton N, Lim S, Large T. Image restoration for under-display camera. Proceedings of the IEEE/CVF Conference on Computer Vision and Pattern Recognition. 2021; 9179–88.

16. Tsai YH, Huang MH, de JW, Huang TW, Lo KL, Ou-Yang M. Image quality affected by diffraction of aperture structure arrangement in transparent active-matrix organic light-emitting diode displays. Appl Optics. 2015;54(28):E136–45.

17. Qin Z, Xie J, Lin FC, Huang YP, Shieh HPD. Evaluation of a transparent Display's pixel structure regarding subjective quality of diffracted see-through images. IEEE Photonics J. 2017; 9(4):7000414.

18. Hecht E. Optics Pearson; 2017.

AUTHOR BIOGRAPHIES

Qian Yang received his BS degree in Physics from Nanjing University in 2017 and MS degree in Physics from University of Rochester in 2019. He is currently working toward a PhD degree from the College of Optics and Photonics, University of Central Florida. His current research interests include liquid crystal spatial light modulators for LiDAR applications, planar optics for AR/VR displays, and miniLED and micro-LED displays.

Zhiyong Yang received his BS degree in Optoelectronic Engineering from Chongqing University in 2017 and is currently working toward a PhD degree from the College of Optics and Photonics, University of Central Florida. His current research interests include various display technologies such as miniLED backlight LCDs, OLED displays, and micro-LED displays.

Yi-Fen Lan received his PhD degree from National Taiwan University in 2010. Currently, he is a principal engineer at AU Optronics Corporation. His research interests include high-dynamic-range LCDs and micro-LED displays. Dr. Yi-Fen Lan is principal engineer at AU Optronics. He received his PhD on Polymer Science from National Taiwan University (2010). He was a visiting scholar at Prof. Shin-Tson Wu's Lab (University of Central Florida, USA) in 2013 and visiting scientist at Prof. Daping Chu's Lab (University of Cambridge, UK) in 2014. His research interests include polymer-stabilized blue phase liquid crystal display and micro-LED display. Presently, he focuses on mass transfer and mass repair of micro-LED manufacturing.
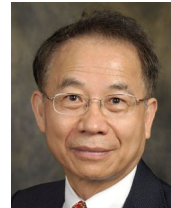
Shin-Tson Wu is a Pegasus professor at College of Optics and Photonics, University of Central Florida. He is the recipient of Optica/IS&T Edwin H. Land medal (2022), SPIE Maria Goeppert Mayer award (2022), OSA Esther Hoffman Beller medal (2014), SID Slottow-Owaki prize (2011), OSA Joseph Fraunhofer award (2010), SPIE G. G. Stokes award (2008), and SID Jan Rajchman prize (2008). In 2014, he was inducted to the inaugural Florida Inventors Hall of Fame. He is a Charter Fellow of the National Academy of Inventors, and a Fellow of the IEEE, OSA, SID, and SPIE. In the past, he served as founding Editor-In-Chief of the IEEE/OSA Journal of Display Technology, OSA Publications Council Chair, OSA Board of Directors, and SID honors and awards committee chair.